Kinetic theory analysis of a gas flow in a square cavity

Masanari Hattori
Department of Aeronautics and Astronautics, Kyoto University

1 Introduction

Consider a flow in a cavity driven by its lid motion. This is a classical problem in fluid mechanics. In particular, the so-called two-dimensional lid-driven cavity flow, where the cavity is an infinitely long rectangular one and the lid moves in the direction normal to its line of contact with the cavity walls, is frequently considered. There has been extensive studies for various purposes (see, e.g., Ref. [1]).

For the flow, the no-slip boundary condition makes the solution singular at the contact point of the moving lid and the resting cavity walls [2]. We call the point a corner hereafter. The flow velocity changes considerably within arbitrarily short distance near the corner. It is multivalued there although it is bounded. Some components of the stress tensor diverge in approaching the corner inversely proportionally to the distance from there. Since the divergence rate is a nonintegrable one, the total forces acting on the lid and the cavity walls diverge too. Their divergence imply that there are some difficulties in the description of the lid-driven cavity flow using conventional fluid mechanics.

Hereafter, we consider a monatomic gas as a fluid. Using the expression of the Stokes solution, we can estimate from how much distance from the corner the fluid-dynamic description becomes unreliable. The estimate tells us that, with ℓ being the mean free path of gas molecules, it is inside the region within $O(\ell)$ from the corner ($r \lesssim \ell$) that the conventional fluid mechanics would fail to describe the behavior correctly. For phenomena with a mean free path scale, the kinetic theory of gases may give a more reliable result.

There are several studies investigating the lid-driven flow in a rectangular cavity based on the kinetic theory (see, e.g., Refs. [3, 4, 5, 6]). These works focus on nonequilibrium effects appearing in the bulk region. Their magnitude is characterized by the Knudsen number, which is defined as the ratio of the mean free path to the cavity size.

However, consideration of the issue of corner singularity based on the kinetic theory seems not to be reported yet, despite the expected advantage of the theory. Under this circumstance, we aim to understand the behavior of the flow velocity and the stress fields

near the corner by the kinetic framework. We consider a slow steady flow in a square cavity, where its lid slides in the direction of its line of contact with the cavity wall. Along whichever direction the lid moves, the corner singularity arises, and the simpler setting allows more accurate observation of the properties of our interest compared to the usual lid-driven cavity flow problem.

This paper is a résumé of a previous study by the author in Ref. [7]. The rest of the paper is organized as follows. In Sec. 2, we state the problem and formulate it. Before proceeding to the numerical results, the properties of the Stokes solution and the free molecular solution are explained in Sec. 3. The numerical results are presented in Section 4. Section 5 concludes the paper.

2 Setting

2.1 Problem

Consider a gas in a cavity with a square cross-section $-L/2 < X_1 < L/2$, $-L/2 < X_2 < L/2$ (X_i are the Cartesian coordinates). The cavity is infinitely long in the X_3 direction. The upper part of the cavity ($X_2 = L/2$) is closed by a planar lid moving at a constant speed $U_{\rm w}$ in the X_3 direction. The cavity walls and the lid are kept at a common uniform temperature T_0. There is no external force. We will investigate the steady behavior of the gas based on the Bhatnagar–Gross–Krook (BGK) equation [8] with the diffuse reflection boundary conditions on the cavity walls and the lid. The lid speed $U_{\rm w}$ is sufficiently smaller than the most probable speed $(2RT_0)^{1/2}$ of gas molecules so that the equation and the boundary condition can be linearized around a uniform equilibrium state at rest with density ρ_0 and temperature T_0 (R is the specific gas constant and ρ_0 is the average density of the gas).

2.2 Basic equation

Let us denote by Lx_i ($i = 1, 2, 3$) the position, by $U_{\rm w} = (2RT_0)^{1/2}u_{\rm w}$ the lid speed, by $(2RT_0)^{1/2}u_i(x_1, x_2)$ the flow velocity, and by $\rho_0 RT_0[\delta_{ij} + P_{ij}(x_1, x_2)]$ the stress tensor, respectively. Here, δ_{ij} is the Kronecker delta.

The problem can be formulated at first as a boundary-value problem of the linearized BGK equation for the velocity distribution function (VDF) of gas molecules, which includes the molecular velocity as its indepedent variables in addition to the position x_i.

Fortunately however, thanks to the structure of the linearized BGK equation and the diffuse reflection boundary condition, they can be further reduced to linear integral equations for the macroscopic quantities (see, e.g., Ref. [9]). We make use of this reduction.

For the present case, as a result, an integral equation for the flow velocity field $u_3(\boldsymbol{x})$ is derived and given as

$$u_3(\boldsymbol{x}) - A[u_3](\boldsymbol{x}) = u_{\rm w} b(\boldsymbol{x}). \tag{1}$$

Here,

$$A[u_3](\boldsymbol{x}) = \frac{1}{k\pi} \int_{\Omega_{\rm R}} \left[G^{(u_3)}(\boldsymbol{x}_* - \boldsymbol{x}) + G^{(u_3)}(\boldsymbol{x}_* - \bar{\boldsymbol{x}}) \right] u_3(\boldsymbol{x}_*) {\rm d}\boldsymbol{x}_*, \tag{2}$$

$$G^{(u_3)}(\boldsymbol{z}) = \frac{1}{|\boldsymbol{z}|} J_0 \left(\frac{|\boldsymbol{z}|}{k} \right), \tag{3}$$

$$b(\boldsymbol{x}) = \frac{1}{\pi} \int_{-1/2}^{1/2} \frac{(1/2 - x_2)}{|\boldsymbol{x}_*^{(\rm U)} - \boldsymbol{x}|^2} J_1 \left(\frac{|\boldsymbol{x}_*^{(\rm U)} - \boldsymbol{x}|}{k} \right) {\rm d}x_{1*}. \tag{4}$$

The positions $\boldsymbol{x} = (x_1, x_2)$ and $\bar{\boldsymbol{x}} = (-x_1, x_2)$, the integration variable $\boldsymbol{x}_* = (x_{1*}, x_{2*})$, and the position $\boldsymbol{x}_*^{(\rm U)} = (x_{1*}, 1/2)$ on the lid are the two-dimensional vectors in the $x_1 x_2$ plane. In (2), ${\rm d}\boldsymbol{x}_* = {\rm d}x_{1*}{\rm d}x_{2*}$. The domain $\Omega_{\rm R}$, appearing in the linear integral operator $A[\cdot]$ given by (2) is the right half of the cavity cross section $0 < x_{1*} < \frac{1}{2}$, $-\frac{1}{2} < x_{2*} < \frac{1}{2}$. The source term $u_{\rm w} b(\boldsymbol{x})$ is given as the integral along the lid surface $x_{2*} = 1/2$ [see (4)]. The functions J_0 and J_1 are the Abramowitz functions defined by

$$J_n(\eta) = \int_0^\infty t^n \exp\left(-t^2 - \frac{\eta}{t} \right) {\rm d}t \quad (\eta \geq 0). \tag{5}$$

The parameter k occurring in (2)–(4) is given by

$$k = \frac{\sqrt{\pi}}{2} {\rm Kn}, \quad {\rm Kn} = \frac{\ell_0}{L}, \quad \ell_0 = \frac{(8RT_0/\pi)^{1/2}}{A_{\rm c}\rho_0}. \tag{6}$$

Here, $A_c \rho_0$ and ℓ_0 are the collision frequency and the mean free path of gas molecules for the BGK model in the equilibrium state at rest with density ρ_0 and temperature T_0 (A_c: constant), and Kn is the Knudsen number. Since the range of integration in $A[u_3]$ is limited to $\Omega_{\rm R}$, the integral equation (1) can be solved in $\Omega_{\rm R}$.

The function $b(\boldsymbol{x})$ in (1) is multivalued at the upper corner $(x_1, x_2) = (1/2, 1/2)$ (its limiting value depends on the direction from which the corner is approached). Then, as expected from the structure of equation (1), the flow velocity component $u_3(\boldsymbol{x})$ can also be multivalued. To deal with the property appropriately, the following plane polar coordinates with their origin at corners, say (σ_+, φ_+) and (σ_-, φ_-), are introduced:

$$x_1 = \frac{1}{2} - \sigma_\pm \cos\varphi_\pm, \quad x_2 = \pm\frac{1}{2} \mp \sigma_\pm \sin\varphi_\pm \quad (0 \leq \varphi_\pm \leq \pi/2). \tag{7}$$

Here, $\sigma_\pm$ is the distance from the top or bottom corner on the right side $(1/2, \pm 1/2) \equiv \boldsymbol{x}_{\rm c}^\pm$ to the point $\boldsymbol{x}$, and $\varphi_\pm$ is an angle of the vector $\boldsymbol{x} - \boldsymbol{x}_{\rm c}^\pm$ measured from $x_2 = \pm 1/2$ to $x_1 = 1/2$. In terms of these coordinates, e.g., the values of $u_3(\boldsymbol{x})$ at the upper right corner

are written as $u_3(\boldsymbol{x}(\sigma_+ = 0, \varphi_+))$. Hence, its possible multivalueness can be appropriately taken into account as its dependence on the angle φ_+.

As for the stress components P_{13} and P_{23}, they are given in terms of u_3 as

$$\begin{aligned}\begin{bmatrix} P_{13}(\boldsymbol{x}) \\ P_{23}(\boldsymbol{x}) \end{bmatrix} =& \frac{1}{k\pi} \int_{\Omega_{\mathrm{R}}} \begin{bmatrix} G^{(P_{13})}(\boldsymbol{x}_* - \boldsymbol{x}) + G^{(P_{13})}(\boldsymbol{x}_* - \bar{\boldsymbol{x}}) \\ G^{(P_{23})}(\boldsymbol{x}_* - \boldsymbol{x}) + G^{(P_{23})}(\boldsymbol{x}_* - \bar{\boldsymbol{x}}) \end{bmatrix} u_3(\boldsymbol{x}_*) \mathrm{d}\boldsymbol{x}_* \\ & - \frac{2u_{\mathrm{w}}}{\pi} \int_{-1/2}^{1/2} \frac{(1/2 - x_2)}{|\boldsymbol{x}_*^{(\mathrm{U})} - \boldsymbol{x}|^2} \begin{bmatrix} (x_{1*} - x_1)|\boldsymbol{x}_*^{(\mathrm{U})} - \boldsymbol{x}|^{-1} J_2\left(|\boldsymbol{x}_*^{(\mathrm{U})} - \boldsymbol{x}|/k\right) \\ (1/2 - x_2)|\boldsymbol{x}_*^{(\mathrm{U})} - \boldsymbol{x}|^{-1} J_2\left(|\boldsymbol{x}_*^{(\mathrm{U})} - \boldsymbol{x}|/k\right) \end{bmatrix} \mathrm{d}x_{1*}, \end{aligned} \tag{8}$$

where

$$G^{(P_{i3})}(\boldsymbol{z}) = -\frac{2z_i}{|\boldsymbol{z}|} J_1\left(\frac{|\boldsymbol{z}|}{k}\right) \quad (i = 1, 2). \tag{9}$$

Once we obtain the unknown flow velocity field u_3, P_{13} and P_{23} can be obtained by (8).

Note that the flow velocity component u_3 and the stress components P_{13} and P_{23} can be considered to be symmetric with respect to $x_1 = 0$, as expected from the geometry and the direction of the lid motion. The u_3 and P_{23} are even and P_{13} is odd with respect to x_1. Also note, in the present problem, that the density and temperature are uniformly ρ_0 and T_0, respectively, that the flow is unidirectional ($u_1 = u_2 = 0$), and that only $P_{13}(= P_{31})$ and $P_{23}(= P_{32})$ are nonzero among the perturbation of the stress.

3 Properties of Stokes and free molecular solutions

Before going to numerical analysis of the integral equation (1), let us explain the Stokes solution and the solution in the free molecular limit ($k \to \infty$) briefly in this section.

3.1 Stokes solution

In the present problem, the Stokes solution can be sought assuming that the flow is unidirectional and there is no pressure gradient. Then, we are led to the Laplace's equation for the flow velocity u_3 in the square domain, $\Delta u_3 = 0$, with the Dirichlet boundary conditions $u_3 = u_{\mathrm{w}}$ (on $x_2 = 1/2$, the lid), $u_3 = 0$ (on $x_2 = -1/2$ or $x_1 = \pm 1/2$, the bottom or side walls). Here Δ is the Laplacian $\Delta = \partial_{x_1}^2 + \partial_{x_2}^2$. The stress components P_{13} and P_{23} are given in terms of u_3 based on the Newton's law:

$$P_{i3}(x_1, x_2) = -k \frac{\partial u_3}{\partial x_i} \quad (i = 1, 2), \tag{10}$$

where k is defined in (6).

To have a quantitatively satisfactory solution, which we shall use later in Sec. 4, we extract the singular part of the solution. We easily see that a simple linear function

$u_{\mathrm{w}}(2/\pi)[(\pi/2) - \varphi_+(\boldsymbol{x})]$ satisfies the Laplace equation in the domain Ω_{R} ($x_1 \geq 0$), the boundary conditions on the lid ($\varphi_+ = 0$) and on the side wall ($\varphi_+ = \pi/2$). (It does not satisfy the condition on the bottom wall.) Hoping that the function well represents the behavior of the flow velocity field u_3 near the upper corner, we decompose u_3 into the following known part $u_3^\dagger$ and unknown part $u_3^\#$:

$$u_3(\boldsymbol{x}) = u_3^\dagger(\boldsymbol{x}) + u_3^\#(\boldsymbol{x}). \tag{11}$$

Here, $u_3^\dagger(\boldsymbol{x})$ is defined as

$$u_3^\dagger(\boldsymbol{x}) = \frac{2u_{\mathrm{w}}}{\pi}\left(\frac{\pi}{2} - \varphi_+(\boldsymbol{x})\right) S(\sigma_+(\boldsymbol{x})) \quad (x_1 \geq 0), \tag{12a}$$

$$S(z) = \frac{e^{-1/(1-2z)}}{e^{-(1/2z)} + e^{-1/(1-2z)}} H\left(\frac{1}{2} - z\right), \tag{12b}$$

where H is the Heaviside function and $u_3^\dagger(x_1, x_2) = u_3^\dagger(-x_1, x_2)$ ($x_1 < 0$). Near the corner, the approximation $u_3^\dagger$ agrees well with the abovementioned function $u_{\mathrm{w}}(2/\pi)[(\pi/2) - \varphi_+(\boldsymbol{x})]$. The unknown part $u_3^\#$ is a solution of the Dirichlet problem of the Poisson's equation, which is derived by substituting the decomposition (11) into the equation and boundary conditions for u_3.

Thanks to the present choice of $u_3^\dagger$, the problem for $u_3^\#$ can be safely handled without singular factors. We solve it numerically by a standard second-order central finite difference scheme. Hence, u_3 for the case of Stokes solution is expressed as a sum of the explicit expression for the singular part and numerical information for the smooth remaining part.

From the numerical result, it can be confirmed that $u_3^\#$ approaches 0 as the corner is approached ($\sigma_+ \to +0$). Meanwhile, $u_3^\dagger|_{\sigma_+=0} = u_{\mathrm{w}}(2/\pi)[(\pi/2) - \varphi_+(\boldsymbol{x})]$ depends on the angle φ_+. Thus, $u_3 (= u_3^\dagger + u_3^\#)$ is multivalued. Now, we introduce the following azimuthal component $P_{\varphi 3}$ of the stress:

$$P_{\varphi 3} = P_{13}\sin\varphi_+ - P_{23}\cos\varphi_+ = -\frac{k}{\sigma_+}\frac{\partial u_3}{\partial \varphi_+}. \tag{13}$$

From (13) and the decomposition (11) of the flow velocity u_3, $P_{\varphi 3}$ can be expressed as

$$P_{\varphi 3} = P_{\varphi 3}^\dagger + P_{\varphi 3}^\#, \quad P_{\varphi 3}^\dagger = -\frac{k}{\sigma_+}\frac{\partial u_3^\dagger}{\partial \varphi_+}, \quad P_{\varphi 3}^\# = P_{13}^\#\sin\varphi_+ - P_{23}^\#\cos\varphi_+, \tag{14}$$

and $P_{13}^\#$ and $P_{23}^\#$ are defined by (10) with u_3 being replaced by $u_3^\#$. Since $\nabla u_3^\#$ is bounded (this can be confirmed from the numerical result), so is $P_{\varphi 3}^\#$. In the meantime, because substituting (12a) into the second equation in (14) leads to the relation

$$P_{\varphi 3}^\dagger = \frac{2k}{\pi\sigma_+} S(\sigma_+) u_{\mathrm{w}} \tag{15}$$

and $S \to 1$ as $\sigma_+ \to +0$, $P^{\dagger}_{\varphi 3}$ and consequently $P_{\varphi 3} (= P^{\dagger}_{\varphi 3} + P^{\#}_{\varphi 3})$ diverge with the rate σ_+^{-1} as $\sigma_+ \to +0$.

The cavity has a corner also on the bottom ($x_1 = 1/2$, $x_2 = -1/2$). The aforementioned singular properties do not appear at this corner $(1/2, -1/2)$ and the solution is smooth including there. The difference in the effect of the corner on the behavior of the gas between top and bottom boundaries stems from that the velocity of the boundaries is discontinuous at the top corner while it is continuous at the bottom one.

3.2 Free molecular solution

In the free molecular limit ($k \to \infty$), the BGK equation (omitted here) reduces to a simple equation, where the effect of intermolecular collision is neglected. This can be easily solved under the diffuse reflection boundary conditions to yield the explict expression of solution at the level of the VDF. Here, we only present the flow velocity and stress fields obtained by taking the moments of the VDF:

$$u_3(\boldsymbol{x}) = \frac{u_{\mathrm{w}}}{2\pi}[\theta_{\mathrm{L}}(\boldsymbol{x}) - \theta_{\mathrm{R}}(\boldsymbol{x})], \tag{16a}$$

$$P_{13}(\boldsymbol{x}) = -\frac{u_{\mathrm{w}}}{2\sqrt{\pi}}[\sin\theta_{\mathrm{L}}(\boldsymbol{x}) - \sin\theta_{\mathrm{R}}(\boldsymbol{x})], \tag{16b}$$

$$P_{23}(\boldsymbol{x}) = \frac{u_{\mathrm{w}}}{2\sqrt{\pi}}[\cos\theta_{\mathrm{L}}(\boldsymbol{x}) - \cos\theta_{\mathrm{R}}(\boldsymbol{x})], \tag{16c}$$

where $\theta_{\mathrm{R}}(\boldsymbol{x})$ and $\theta_{\mathrm{L}}(\boldsymbol{x})$ are the angles of the vectors $(1/2 - x_1, 1/2 - x_2)$ and $(-1/2 - x_1, 1/2 - x_2)$, respectively. They are measured counterclockwise from the x_1 direction. Note that $\theta_{\mathrm{R}}(\boldsymbol{x}) = \varphi_+(\boldsymbol{x})$. From (16a), $u_3(\boldsymbol{x})/u_{\mathrm{w}}$ is equal to the proportion of the contribution of molecules coming from the moving lid surface ($x_2 = 1/2$) over that of the whole molecules, when measured by the range of angle.

As is clear from (16b) and (16c), the stress is bounded for the free molecular solution, which contrasts with the Stokes solution [see the paragraph including (15)]. Because $\theta_{\mathrm{R}}(\boldsymbol{x}) = \varphi_+(\boldsymbol{x})$ and $\theta_{\mathrm{L}}(\boldsymbol{x}) \to \pi$ as $\sigma_+ \to +0$, from (16a),

$$u_3(\boldsymbol{x}) \to \frac{u_{\mathrm{w}}}{2\pi}[\pi - \varphi_+(\boldsymbol{x})] \quad \text{as } \sigma_+ \to +0. \tag{17}$$

Hence, the flow velocity u_3 is multivalued at the corner also in the free molecular solution. The multivalueness emerges because u_3 is determined by the proportion of the contribution of the molecules coming from the lid which depends on the azimuthal angle φ_+, and this feature remains the same when the corner is approached ($\sigma_+ \to +0$). The gradient of u_3 in the φ_+ direction, i.e., $\sigma_+^{-1}\partial_{\varphi_+} u_3$, diverges as $\sigma_+ \to +0$. It should be noted that this divergence does not contradict the boundedness of the stress because the stress is not expressed by the velocity gradient in the kinetic framework.

4 Numerical results and discussions

We solve the integral equation (1) by successive approximation. A sequence $\{u_3^n\}$ by the recurrence formula

$$u_3^n(\boldsymbol{x}) = A[u_3^{n-1}](\boldsymbol{x}) + u_{\rm w} b(\boldsymbol{x}) \quad (n = 1, 2, ...) \tag{18}$$

is considered, starting from some initial guess $u_3^0(\boldsymbol{x})$. As the limit of the sequence, the solution of (1) is obtained. The actual numerical computation based on (18), involving a numerical approximation for the integral $A[u_3^{n-1}]$, is carried out basically by following Refs. [10, 11, 12].

4.1 Macroscopic quantities in the vicinity of corner

As the main interest lies in the fluid-dynamic circumstances and the behavior of the gas near the corner, we focus on cases for small Knudsen numbers. For the sake of consiseness, putting aside the behavior of the gas in overall region, here we examine the behavior of the gas near the corner from the beginning. First, let us focus on the case for $k = 0.01$. We show in Fig. 1 the contour plots of the macroscopic quantities $u_3/u_{\rm w}$, $P_{13}/u_{\rm w}$, and $P_{23}/u_{\rm w}$ in the region $0.45 \le x_{1,2} \le 0.5$ for both the Stokes and the BGK solutions.

For the Stokes solution, the contour lines of $u_3/u_{\rm w}$ are emitted radially from the corner [Fig. 1(a)]. There is no contour line impinging to the lid ($x_2 = 1/2$) and the side wall ($x_1 = 1/2$) since the solution is constant along the surfaces owing to the no-slip condition. On the other hand, for the BGK solution [Fig. 1(d)] some contour lines impinge to the boundaries. Although the considered Knudsen number is fairly small ($k = 0.01$), the results show that the kinetic theory gives a fairly different result compared to the Stokes solution. The magnitude of velocity slip is larger than 0.2 over some parts of the lid ($0.49 \lesssim x_1 \le 0.5$, $x_2 = 1/2$) and the side wall ($0.49 \lesssim x_2 \le 0.5$, $x_1 = 1/2$). This is evidently larger than the magnitude of the slip observed over positions away from the corner, which is $O(k)$ [see, e.g., the plots over $\sigma_+ \ge 0.2$ in Figs. 2(a) shown later].

Figures 1(b) and 1(c) show the stress components for the Stokes solution. The contour lines which are the closest to the corner are the ones with the maximum magnitude level among the drawn lines (the corresponding values are $P_{13}/u_{\rm w} = 0.45$, $P_{23}/u_{\rm w} = -0.6$). In the regions enclosed by these lines and the boundaries, the magnitude of P_{13} and P_{23} increases infinitely as the corner is approached as explained in the paragraph including (15) in Sec. 3.1. In contrast to this, for the BGK solution, P_{13} and P_{23} are bounded [see Figs. 1(e) and 1(f)] as in the free molecular limit in Sec. 3.2. The magnitudes of $P_{13}/u_{\rm w}$ and $P_{23}/u_{\rm w}$ are both less than 0.445 in the whole region including the corner. Hence, although what we examine here is the result for only one specific case $k = 0.01$, it implies

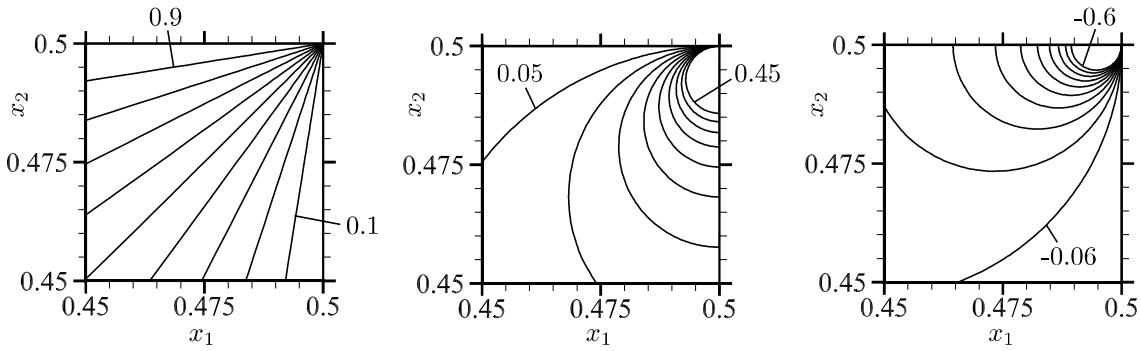

(a) $u_3/u_{\rm w}$ (Stokes) (b) $P_{13}/u_{\rm w}$ (Stokes) (c) $P_{23}/u_{\rm w}$ (Stokes)

(d) $u_3/u_{\rm w}$ (BGK) (e) $P_{13}/u_{\rm w}$ (BGK) (f) $P_{23}/u_{\rm w}$ (BGK)

Fig. 1: Contour plots of the macroscopic quantities near the corner $(1/2, 1/2)$ for the Stokes and BGK solutions with $k = 0.01$. (a) $u_3/u_{\rm w}$ (Stokes), (b) $P_{13}/u_{\rm w}$ (Stokes), (c) $P_{23}/u_{\rm w}$ (Stokes), (d) $u_3/u_{\rm w}$ (BGK), (e) $P_{13}/u_{\rm w}$ (BGK), and (f) $P_{23}/u_{\rm w}$ (BGK). The curves are drawn with intervals 0.1, 0.05, and 0.06 in (a) and (d), (b) and (e), and (c) and (f), respectively.

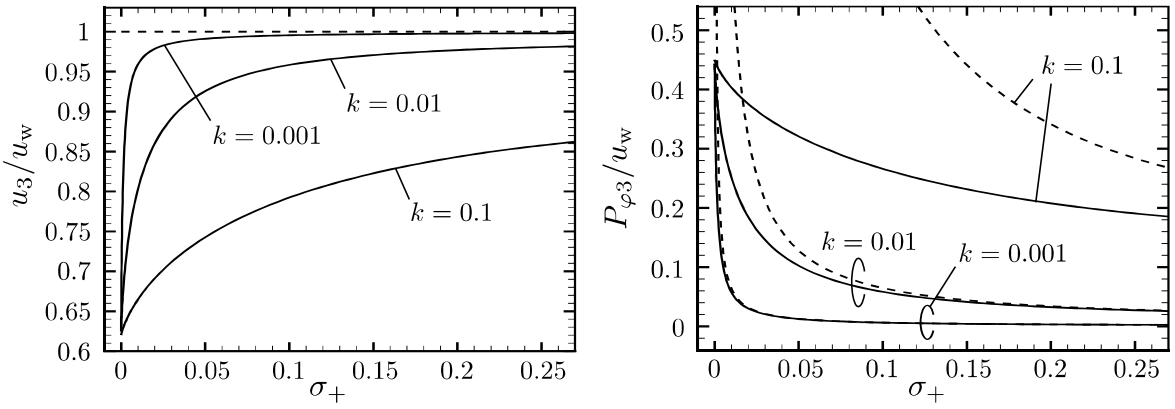

(a) $u_3/u_{\rm w}$ (b) $P_{\varphi 3}/u_{\rm w}$

Fig. 2: Profiles of flow velocity and shear stress near the corner $(1/2, 1/2)$ for $k = 0.1$, 0.01, and 0.001. $\varphi_+ = 0$. (a) $u_3/u_{\rm w}$ and (b) $P_{\varphi 3}/u_{\rm w}$. The solid and dashed lines indicate the BGK and Stokes solutions, respectively. The quantities are plotted as functions of σ_+, the distance from the corner.

that the problem of stress divergence for the Stokes solution is resolved in the description based on the kinetic theory.

In Fig. 2, we show the flow velocity and the stress for $k = 0.1$, 0.01, and 0.001 along the direction of the angle $\varphi_+ = 0$ (the lid surface) as functions of the distance σ_+. As for the stress, its azimuthal component $P_{\varphi 3}$ associated with the coordinates (σ_+, φ_+) is plotted [see also (13) and $P_{\varphi 3} = -P_{23}$ $(\varphi_+ = 0)$]. From Fig. 2(a), it is seen that, while $u_3/u_{\rm w}$ for $\varphi_+ = 0$ approaches toward the value unity of the Stokes solution due to the no-slip condition in overall region as k decreases, it approaches to another value 0.625... near $\sigma_+ = 0$ for the cases with any k shown in the figures. While the stress $P_{\varphi 3}/u_{\rm w}$ is $O(k)$ for large σ_+ and also agrees well with the Stokes solution for $k = 0.01$ and 0.001 [Fig. 2(b)], the BGK solution approaches another $O(1)$ value 0.443... near $\sigma_+ = 0$ for the cases with any k shown in the figures. The results imply that the magnitude of velocity slip and stress remains $O(1)$ near the corner indepedent of k. Note that corresponding properties can be confirmed for the side wall as well.

The spatial variations of the macroscopic quantities observed in Fig. 2 can be understood clearer by changing a length scale used in plots from the cavity size to a length of the order of the mean free path. With such a length scale, $u_3/u_{\rm w}$ and $P_{\varphi 3}/u_{\rm w}$ with $\varphi_+ = 0$ are plotted again in Figs. 3(a) and (b). The plot curves for various k converge to a common place as k decreases. This indicates the variation of a mean free path scale near the corner when the Knudsen number is small.

Before closing this subsection, to examine if the flow velocity is multivalued or not, we

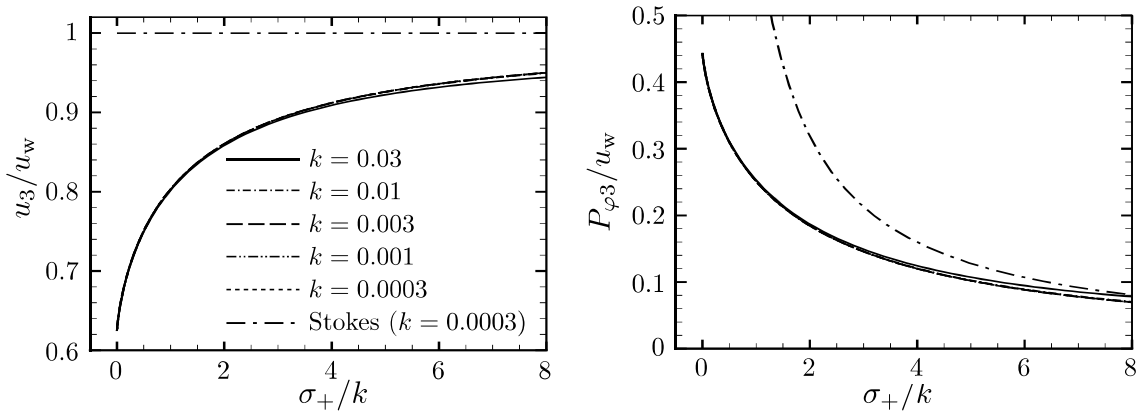

(a) u_3/u_w (b) $P_{\varphi 3}/u_\mathrm{w}$

Fig. 3: Plots of macroscopic quantities on the lid ($\varphi_+ = 0$) for $k = 0.03$, 0.01, 0.003, 0.001, and 0.0003. The quantities are plotted as functions of σ_+/k, the rescaled distance from the corner $(1/2, 1/2)$. (a) u_3/u_w and (b) $P_{\varphi 3}/u_\mathrm{w}$. The types of lines used are common in (a) and (b) and see the line legend in (a).

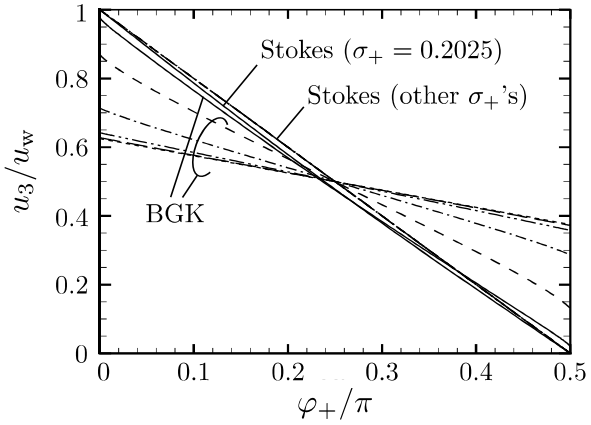

Fig. 4: Profiles of flow velocity for the BGK and Stokes solutions with $k = 0.01$. The quantities are plotted as functions of the azimuthal angle φ_+ with σ_+, the distance from the corner $(1/2, 1/2)$, being fixed. The solid, dashed, dash-dotted, dash-double-doted, long-dashed, and dotted lines indicate the results for $\sigma_+ = 0.2025$, 0.02260, 2.771×10^{-3}, 2.770×10^{-4}, 2.778×10^{-5}, and 0, respectively.

show u_3/u_w for $k = 0.01$ as functions of the angle φ_+ with the distance σ_+ being fixed at several values in Fig. 4. The slope of curves for the BGK solution is small due to the velocity slip compared to the Stokes solution. However, the plot curves for the former also converge to the nonconstant profile as $\sigma \to +0$. This demonstrates that the flow velocity is multivalued not only in the Stokes solution but also in the kinetic solution.

The origin of the multivalueness is essentially similar to that of the free molecular solution, which was explained in the last paragraph of Sec. 3.2. we explain the reason below. The flow velocity component consists of $A[u_3]$ and $u_\mathrm{w}b$: $u_3(\boldsymbol{x}) = A[u_3](\boldsymbol{x}) + u_\mathrm{w}b(\boldsymbol{x})$ [see (1)]. At the corner $(x_1, x_2) = (1/2, 1/2)$, $A[u_3](\boldsymbol{x})$ is not multivalued, which can be confirmed with the aid of the numerical results. On the other hand, for $b(\boldsymbol{x})$ [see (4)], by the change of variable from x_{1*} to ψ as $x_{1*} - x_1 = (1/2 - x_2)/\tan\psi$, we have

$$\begin{aligned} b(\boldsymbol{x}) =& \frac{1}{\pi}\int_{\theta_\mathrm{R}(\boldsymbol{x})}^{\theta_\mathrm{L}(\boldsymbol{x})} J_1\left(\frac{1/2 - x_2}{k\sin\psi}\right)\mathrm{d}\psi \\ =& \frac{1}{\pi}\int_{\varphi_+}^{\theta_\mathrm{L}(\boldsymbol{x})} J_1\left(\frac{\sigma_+\sin\varphi_+}{k\sin\psi}\right)\mathrm{d}\psi \\ \to& \frac{1}{\pi}\int_{\varphi_+}^{\pi} J_1(0)\,\mathrm{d}\psi = \frac{\pi - \varphi_+(\boldsymbol{x})}{2\pi} \quad (\text{as } \sigma_+ \to +0). \end{aligned} \tag{19}$$

In (19), we used that $\theta_\mathrm{L}(\boldsymbol{x}) \to \pi$ in taking the limit[1] $\sigma_+ \to +0$ and that $J_1(0) = 1/2$. From (19), $u_\mathrm{w}b(\boldsymbol{x})$ is identical to the free molecular solution (17). This accords with the situation that the molecules coming from the lid to the corner do not experience intermolecular collision.

4.2 Forces exerted on lid and cavity walls

We denote by $\rho_0 RT_0 u_\mathrm{w} L F_\mathrm{U}$, $\rho_0 RT_0 u_\mathrm{w} L F_\mathrm{B}$, and $\rho_0 RT_0 u_\mathrm{w} L F_\mathrm{R}$ the total forces in the X_3 direction per unit length in X_3 exerted on the lid, the bottom wall, and the right side wall, respectively. Then, F_U, F_B, and F_R are written as

$$u_\mathrm{w}F_\mathrm{U} = \int_{-\frac{1}{2}}^{\frac{1}{2}} P_{23}(x_1, \frac{1}{2})\mathrm{d}x_1, \quad u_\mathrm{w}F_\mathrm{B} = -\int_{-\frac{1}{2}}^{\frac{1}{2}} P_{23}(x_1, -\frac{1}{2})\mathrm{d}x_1, \quad u_\mathrm{w}F_\mathrm{R} = \int_{-\frac{1}{2}}^{\frac{1}{2}} P_{13}(\frac{1}{2}, x_2)\mathrm{d}x_2. \tag{20}$$

[1] Since both the denominator $k\sin\psi$ and the numerator $\sigma_+\sin\varphi_+$ of the argument of J_1 tend to 0 as $\sigma_+ \to +0$ and $\psi \to \theta_\mathrm{L}(\boldsymbol{x})$, care should be taken in taking the limit $\sigma_+ \to +0$. The result in (19) can be justified, for example, as follows. To begin with, $\theta_\mathrm{L}(\boldsymbol{x})$ can be expressed as $\theta_\mathrm{L} = \pi - \alpha$ with $\alpha = \tan^{-1}(\sigma_+\sin\varphi_+/(1 - \sigma_+\cos\varphi_+))$. Take another angle $\beta = \tan^{-1}(\sqrt{\sigma_+}\sin\varphi_+/(1 - \sigma_+\cos\varphi_+))$, which is larger than α and tends to 0 as $\sigma_+ \to +0$. Then, split the integral as $b(\boldsymbol{x}) = \pi^{-1}\int_{\varphi_+}^{\pi-\alpha} J_1\mathrm{d}\psi = \pi^{-1}\int_{\varphi_+}^{\pi-\beta} J_1\mathrm{d}\psi + \pi^{-1}\int_{\pi-\beta}^{\pi-\alpha} J_1\mathrm{d}\psi$. Thanks to the choice of β, in the first integral, where $\varphi_+ < \psi < \pi - \beta$, the argument of J_1 approaches 0 uniformly as $\sigma_+ \to +0$. Thus, it approaches the result in (19). On the other hand, we see that the second integral tends to 0 because its magnitude is bounded from above by $\pi^{-1}J_1(0)(\beta - \alpha)$ [$J_1(0)$ is the maximum of the function J_1] and $\alpha, \beta \to 0$ as $\sigma_+ \to +0$.

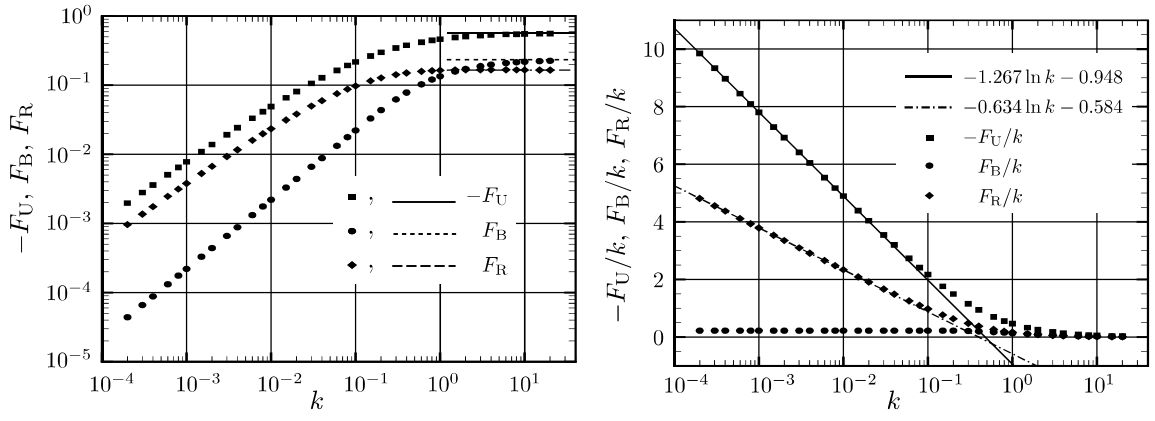

(a) $(-F_{\mathrm{U}}, F_{\mathrm{B}}, F_{\mathrm{R}})$ in log-log plot

(b) $(-F_{\mathrm{U}}/k, F_{\mathrm{B}}/k, F_{\mathrm{R}}/k)$ in semilog plot

Fig. 5: The forces acting on the lid and the cavity walls. Plots related to F_{U}, F_{B}, and F_{R} as functions of k. (a) $(-F_{\mathrm{U}}, F_{\mathrm{B}}, F_{\mathrm{R}})$ in log-log plot and (b) $(-F_{\mathrm{U}}/k, F_{\mathrm{B}}/k, F_{\mathrm{R}}/k)$ in semilog plot. Horizontal lines in (a) indicate the free molecular solution, $(-F_{\mathrm{U}}, F_{\mathrm{B}}, F_{\mathrm{R}})|_{k\to\infty} = (1, \sqrt{2}-1, 1-1/\sqrt{2})/\sqrt{\pi}$, which is obtained from (16b) and (16c).

In order to examine the forces for small Knudsen numbers, we show F_{U}, F_{B}, and F_{R} as functions of k in Fig. 5(a) with a log-log plot. The force F_{B} exerted on the bottom wall is actually proportional to k. This F_{B} can be also recovered satisfactorily by the Stokes solution in Sec. 3.1. The Stokes equation under the no-slip condition can predict well the force exerted on the bottom wall although the bottom wall meets corners between it and the side walls. The effect of corners on the behavior of the gas is rather weak on the bottom side.

From Fig. 5(a), on the other hand, it is found that F_{U} and F_{R} are not proportional to k. In order to find the dependence of F_{U} and F_{R} on k, another plot is shown in Fig. 5(b). As k decreases, $-F_{\mathrm{U}}/k$ and F_{R}/k increase, and the markers are nearly on the straight lines in the figure. This means that F_{U} and F_{R} behave like $k \ln k$ for small k.

We consider why the forces F_{U} and F_{R} behave as $k \ln k$. In Fig. 6(a), the stress on the lid is shown with a log-log plot. The results for $k = 0.1$, 0.01, 0.001, and 0.0003 are shown. For small k, the magnitude of the stress grows up inversely proportionally to σ_+ over a wide range from around $\sigma_+ = 0.1 \sim 0.2$ to the neighborhood of the corner. This is the fluid-dynamic behavior of the stress confirmed in the paragraph including (15) in Sec. 3.1. Figure 6(b) shows another plot with the distance σ_+ being rescaled by k. The curves for the BGK model overlap well up to larger σ_+/k as k becomes smaller and the Stokes solution agrees well with the BGK solution up to $\sigma_+/k = 10$ or 20. Figures 6(a)(b) imply that the BGK solution increases inversely proportionally to the distance from the corner over the range from comparatively far position to the position that is a few tens of mean

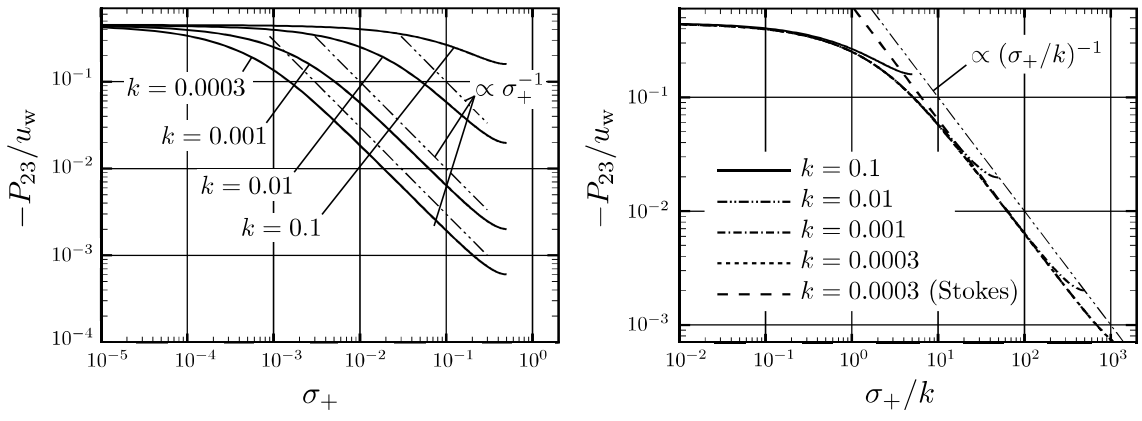

(a) σ_+ vs $-P_{23}/u_{\mathrm{w}}$ (b) σ_+/k vs $-P_{23}/u_{\mathrm{w}}$

Fig. 6: Profiles of shear stress on the lid. In (a) and (b), they are shown as a function of σ_+ and σ_+/k, the distance from the corner and the rescaled one, respectively.

free paths away from there (for example, $\sigma_+ = ck$ with $c = 10$ or 20). Then, consider the integral of k/σ_+ on the interval read from the above observations, i.e., on $ck < \sigma_+ < x_0$ (x_0 is, e.g., 0.1 or 0.2). The factor $k \ln k$ occurs as $\int_{ck}^{x_0} (k/\sigma_+) d\sigma_+ = -k \ln(ck) + k \ln(x_0)$. Hence, $k \ln k$ appears because of the continuation of the abovementioned fluid-dynamic stress increase up to the position that is only a few tens of mean free paths away from the corner and of the subsequent transition to another bounded profile at positions closer to the corner.

5 Concluding remarks

We considered a gas flow in a square cavity driven by a lid sliding in the direction of its line of contact with the cavity walls. The problem was formulated as the boundary-value problem of the linearized BGK equation under the diffuse reflection boundary condition and it was reduced to the integral equation for the flow velocity field that is suitable for an accurate analysis. Applying the Stokes equation with the no-slip boundary condition, the flow velocity becomes multivalued at the corner between the lid and the cavity wall and the shear stress diverges there inversely proportionally to the distance from the corner. For the free molecular solution, first, the flow velocity is still multivalued because the flow velocity is determined by the proportion of the molecules coming from the lid over that of the whole molecules that depends on the azimuthal angle measured from the corner, and this feature remains the same when the corner is approached. Second, the shear stress and accordingly the forces exerted on the lid and the cavity walls are bounded. The two properties were common in the numerical results for the small Knudsen numbers, which

correspond to the usual fluid-dynamic circumstances. The second property implies that the difficulty in the case of the Stokes equation is resolved by using the kinetic approach. The shear stresses given by the Stokes solution and the BGK one for small Knudsen numbers agree well with each other up to the position that is a few tens of mean free paths away from the corner. Within the region, the shear stress varies inversely proportionally to the distance from the corner. At positions closer to the corner, the increase of the stress is suppressed and its magnitude remains bounded for the BGK solution. According to these behavior of the shear stress, the total forces acting on the lid and the side cavity wall behave as $k \ln k$ ($k \ll 1$), where $k[= (2/\sqrt{\pi})\mathrm{Kn}]$ is a parameter corresponding to the Knudsen number Kn.

Acknowledgments

The present work was supported in part by JSPS KAKENHI Grant Nos. 21K14076 and 24K07302.

References

[1] P. N. Shankar and M. D. Deshpande, "Fluid mechanics in the driven cavity," Annu. Rev. Fluid Mech. **32**, 93–136 (2000).

[2] H. K. Moffatt, "Singularities in fluid dynamics and their resolution," in *Lectures on Topological Fluid Mechanics*, edited by R. L. Ricca (Springer, Berlin, Heidelberg, 2009), pp. 157–166.

[3] S. Naris and D. Valougeorgis, "The driven cavity flow over the whole range of the Knudsen number," Phys. Fluids **17**, 097106 (2005).

[4] B. John, X.-J. Gu, and D. R. Emerson, "Investigation of heat and mass transfer in a lid-driven cavity under nonequilibrium flow conditions," Numer. Heat Transfer, Part B **58**, 287–303 (2010).

[5] L. Wu, J. M. Reese, and Y. Zhang, "Oscillatory rarefied gas flow inside rectangular cavities," J. Fluid Mech. **748**, 350–367 (2014).

[6] A. Frezzotti, G. P. Ghiroldi, and L. Gibelli, "Solving the Boltzmann equation on GPUs," Comput. Phys. Commun. **182**, 2445–2453 (2011).

[7] M. Hattori, "Numerical analysis of a gas flow in a square cavity driven by spanwise lid motion on the basis of kinetic theory: Behavior of the gas near a sharp corner," Phys. Fluids **36**, 052006 (2024).

[8] P. L. Bhatnagar, E. P. Gross, and M. Krook, "A model for collision processes in gases. I. small amplitude processes in charged and neutral one-component systems," Phys. Rev. **94**, 511–525 (1954).

[9] Y. Sone, *Molecular Gas Dynamics* (Birkhäuser, Boston, 2007). Supplementary Notes and Errata is available from Kyoto University Research Information Repository. http://hdl.handle.net/2433/66098.

[10] M. Hasegawa and Y. Sone, "Poiseuille and thermal transpiration flows of a rarefied gas for various pipes," J. Vac. Soc. Jpn. **31**, 416–419 (1988).

[11] K. Aoki, Y. Sone, and T. Yano, "Numerical analysis of a flow induced in a rarefied gas between noncoaxial circular cylinders with different temperatures for the entire range of the Knudsen number," Phys. Fluids A **1**, 409–419 (1989).

[12] S. Taguchi and P. Charrier, "Rarefied gas flow over an in-line array of circular cylinders," Phys. Fluids **20**, 067103 (2008).

Department of Aeronautics and Astronautics
Graduate School of Engineering, Kyoto University
Kyoto 615-8540
JAPAN
E-mail address: `hattori.masanari.4r@kyoto-u.ac.jp`